

BPS solitons with internal structures in a restricted baby Skyrme-Maxwell theory in a magnetic medium

J. Andrade,^{1,*} R. Casana,^{1,†} E. da Hora,^{2,‡} and André C. Santos^{1,§}

¹*Departamento de Física, Universidade Federal do Maranhão, 65080-805, São Luís, Maranhão, Brazil.*

²*Coordenação do Curso de Bacharelado Interdisciplinar em Ciência e Tecnologia, Universidade Federal do Maranhão, 65080-805, São Luís, Maranhão, Brazil.*

We consider a restricted baby Skyrme-Maxwell scenario enlarged via the inclusion of a nontrivial magnetic permeability. We then proceed with the minimization of its total energy by means of the Bogomol'nyi-Prasad-Sommerfield (BPS) prescription, from which we get that the self-dual potential now depends on the magnetic permeability itself. As a result, we obtain not only the lower bound for the energy, but also the self-dual equations whose solutions saturate that bound. In such a context, we focus our attention on those time-independent gauged skyrmions with radial symmetry and no electric charge. We solve the effective self-dual equations numerically for different choices of magnetic permeability, from which we obtain BPS magnetic fields whose internal structures form concentric rings. We also explain analytically the formation of these structures based on the values of a single real parameter which characterizes the respective magnetic permeabilities.

PACS numbers: 11.10.Kk, 11.10.Lm, 11.27.+d

I. INTRODUCTION

Topologically nontrivial structures are commonly described by means of those time-independent solutions which come from highly nonlinear Euler-Lagrange equations [1]. In such a context, the potential term which defines the vacuum manifold of the respective theory not only introduces the nonlinearity itself, but it is also expected to allow the spontaneous symmetry breaking mechanism to occur (whose effects include the formation of a topological profile as a result of the corresponding phase transition). The point is that highly nonlinear equations of motion are typically quite hard to solve. However, this issue can be circumvented via the minimization of the system's total energy by employing the Bogomol'nyi-Prasad-Sommerfield (BPS) prescription [2]. The implementation of such algorithm determines a specific expression for the potential, but it also provides a lower bound for the energy (the BPS bound) and the corresponding BPS equations whose solutions saturate that bound (and therefore describe energetically stable configurations). In addition, it is always possible to verify that the BPS equations are compatible with the Euler-Lagrange equations, from which one concludes that the BPS profiles stand for legitimate solutions of the model. In the literature, there are alternative methods for the obtainment of such BPS configurations; see, for instance, the study of the conservation of the energy-momentum tensor [3], the on-shell procedure [4], and the strong-necessary conditions technique [5].

The full Skyrme model was proposed in 1961 as a generalized nonlinear sigma theory defined in $(3 + 1)$ -

dimensions [6]. Its Lagrange density contains the so-called Skyrme term (a quartic kinetic, i.e. a term of degree four in the first-derivative of the scalar sector), the σ term (a quadratic kinetic one), and a potential (a nonderivative term) which was originally proposed in order to study the pion mass. The Skyrme theory can be interpreted as an effective low-energy model of Quantum Chromodynamics which engenders stable solitonic structures, so-called skyrmions, which can be applied to study some physical properties of those hadrons and nuclei [7].

In this context, the study of the planar version of the Skyrme theory, known as the baby Skyrme model [8], serves to the comprehension of many aspects of the original $(3+1)$ -dimensional scenario, including the conditions under which it eventually accepts the implementation of the BPS prescription. The baby Skyrme model in the absence of the σ -term, named the restricted baby Skyrme model [9], supports a BPS structure [10]. Furthermore, over the last years to investigate other physical phenomena, the skyrmions have also been used to describe topological quantum Hall effect [11], in chiral nematic liquid crystals [12], superconductors [13], brane cosmology [14], magnetic materials [15], for instance.

Moreover, in order to investigate the electromagnetic properties of the baby Skyrme model, it is necessary to couple it to an Abelian gauge field [16]. In such a context, the BPS skyrmions appear in a restricted baby Skyrme-Maxwell model [17], and also occur when the Skyrme sector is minimally coupled to the Chern-Simons term [18] and to the Maxwell-Chern-Simons action [19]. Additional results on the study of those BPS solutions in a Skyrme-Born-Infeld scenario can be found in [20], while supersymmetric extensions of these restricted gauged baby Skyrme theories are in the Refs. [21–25].

We now go a little bit further into this issue and consider how the electromagnetic properties of a material medium affect the first-order skyrmions which arise from a BPS restricted baby Maxwell-Skyrme mode. Here,

* joao.luis@discente.ufma.br

† rodolfo.casana@ufma.br

‡ carlos.hora@ufma.br

§ andre.cs@discente.ufma.br

these properties are studied via the introduction of a nonstandard function which multiplies the Maxwell term and therefore represents the magnetic permeability of the medium.

In order to present our results, this manuscript is organised as follows. In the Section II, we introduce the restricted baby Maxwell-Skyrme model enlarged via the inclusion of a nontrivial magnetic permeability. We also present the definitions and conventions which we adopt in our work. In the sequence, we focus our attention on those radially symmetric time-independent profiles which describe gauged skyrmions in a planar context. We then look for first-order solutions via the minimization of the effective total energy by means of the BPS prescription, from which it arises a differential constraint whose solution is the expression for the potential which supports the existence of well-behaved first-order configurations. As a result of our construction, we obtain not only the BPS bound itself, but also the first-order BPS equations which saturate it. Then, in the Sec. III, we use the first-order expressions obtained previously to define effective BPS scenarios and their corresponding gauged skyrmions. The point is that both the potential and the first-order equations depend on the expression for the magnetic permeability explicitly. We then choose such expression in order to generate BPS skyrmions with internal structures, i.e. which behave standardly near the boundaries, but exhibit a nonusual profile in the intermediate regions. In particular, we investigate in detail how the shape of the magnetic field depends on a free real parameter which enters the expression for the magnetic permeability. We generalize these results by choosing a magnetic permeability which gives rise to BPS gauged skyrmions with a much more sophisticated internal structure. In this case, the description of the magnetic profile additionally requires the application of numerical techniques. However, even in this more intricate case, our predictions fit the solutions extremely well. Finally, the Sec. IV brings our ending comments and perspectives regarding future contributions.

In this manuscript, we adopt the natural units system and $\eta^{\mu\nu} = (+ - -)$ for the metric signature, for the sake of simplicity.

II. THE RESTRICTED GAUGED BABY SKYRME IN A MAGNETIC MEDIUM: THE BPS STRUCTURE

We begin by presenting the $(2 + 1)$ -dimensional restricted gauged baby Skyrme model enlarged via the inclusion of an a priori arbitrary function which represents a nontrivial magnetic permeability, the corresponding Lagrangian function reading

$$L = E_0 \int d^2\mathbf{x} \mathcal{L}, \quad (1)$$

where the factor E_0 sets the energy scale of the model (which will be taken as $E_0 = 1$ hereafter). The Lagrangian density is

$$\mathcal{L} = -\frac{G}{4g^2} F_{\mu\nu} F^{\mu\nu} - \frac{\lambda^2}{4} (D_\mu \vec{\varphi} \times D_\nu \vec{\varphi})^2 - V, \quad (2)$$

where the first term stands for Maxwell's action now multiplied by a magnetic permeability function $G = G(\varphi_n)$ which depends on the quantity $\varphi_n = \hat{n} \cdot \vec{\varphi}$. In the internal space, \hat{n} represents an unitary vector which defines a preferred direction, while the Skyrme field $\vec{\varphi} = (\varphi_1, \varphi_2, \varphi_3)$ is given as a triplet of real scalar fields constrained to satisfy $\vec{\varphi} \cdot \vec{\varphi} = 1$ and therefore describing a spherical surface with unitary radius. Moreover, $F_{\mu\nu} = \partial_\mu A_\nu - \partial_\nu A_\mu$ is the electromagnetic field strength tensor and

$$D_\mu \vec{\varphi} = \partial_\mu \vec{\varphi} + A_\mu \hat{n} \times \vec{\varphi} \quad (3)$$

stands for the usual covariant derivative of the Skyrme field. The third term brings the self-interacting potential $V = V(\varphi_n)$, while both λ and g are coupling constants inherent to the model (which we assume to be nonnegative from now on). Moreover, the Skyrme field and the function G are dimensionless, while the gauge field, the electromagnetic constant g and the Skyrme one λ have mass dimensions equal to 1, 1 and -1 , respectively.

It is instructive to write down the Euler-Lagrange equation for the gauge sector which comes from (2), i.e.

$$\partial_\nu (GF^{\nu\mu}) = g^2 j^\mu, \quad (4)$$

where $j^\mu = \hat{n} \cdot J^\mu$ is the conserved current density, with

$$J^\mu = \lambda^2 [\vec{\varphi} \cdot (D^\mu \vec{\varphi} \times D^\nu \vec{\varphi})] D_\nu \vec{\varphi}. \quad (5)$$

The Gauss law for time-independent configurations reads

$$\partial_i (G\partial^i A^0) = g^2 j^0, \quad (6)$$

where

$$j^0 = \lambda^2 A_0 (\hat{n} \cdot \partial^i \vec{\varphi}) (\hat{n} \cdot \partial_i \vec{\varphi}) \quad (7)$$

is the electric charge density. The point is that $A^0 = 0$ stands for a legitimate gauge choice, given that it solves the Gauss law (6) identically. Thus, we conclude that the stationary configurations we study in this manuscript are electrically neutral (i.e. present no electric field and electric charge).

Instead of studying the solutions of the second-order Euler-Lagrange equations, we focus our attention on those first-order configurations which minimize the total energy of the theory. We achieve such a goal via the implementation of the BPS procedure, the starting point being the stationary energy density, which is related to the energy-momentum tensor of the model (2), i.e.

$$T_{\alpha\beta} = -\frac{G}{g^2} F_{\mu\alpha} F^\mu{}_\beta - \lambda^2 (D_\mu \vec{\varphi} \times D_\alpha \vec{\varphi}) \cdot (D^\mu \vec{\varphi} \times D_\beta \vec{\varphi}) - \eta_{\alpha\beta} \mathcal{L}. \quad (8)$$

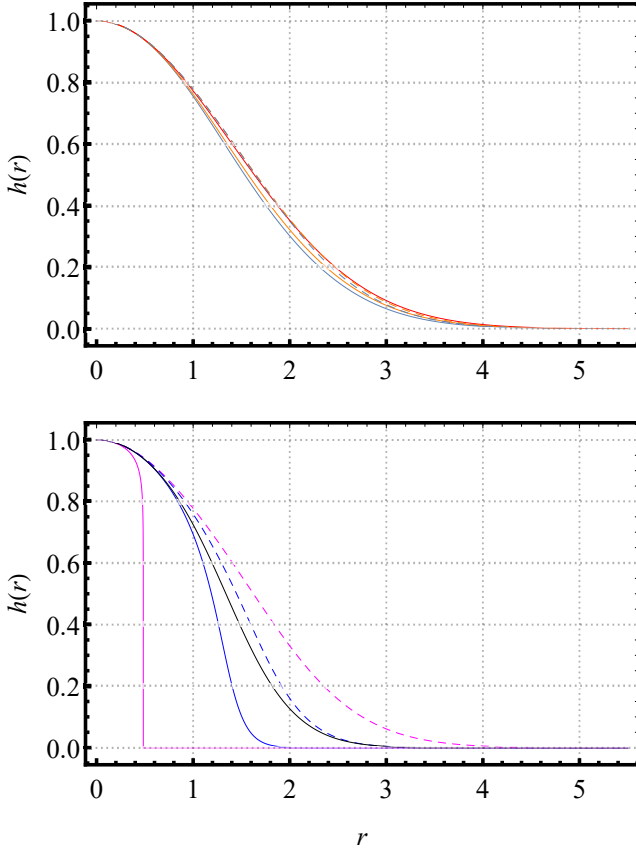


FIG. 1. Numerical solutions to the Skyrme profile function $h(r)$ obtained from Eqs. (45) and (46) for different values of α . Top: $\alpha = 0.15$ (solid navy line), $\alpha = 0.25$ (solid orange line), $\alpha = 0.50$ (solid red line), $\alpha = 0.75$ (dashed orange line) and $\alpha = 0.85$ (dashed navy line). Bottom: $\alpha = 1.0$ (dashed magenta line), $\alpha = 1.5$ (dashed blue line), $\alpha = 2.0$ (solid blue line) and $\alpha = 4.0$ (solid magenta line). The usual solution appears as a solid black line, for comparison.

Thus, the energy density for time-independent fields reads

$$\varepsilon = -\mathcal{L}, \quad (9)$$

which can be written explicitly as (here, we have already implemented $A_0 = 0$)

$$\varepsilon = \frac{G}{2g^2}B^2 + \frac{\lambda^2}{2}Q^2 + V, \quad (10)$$

where the function $Q \equiv \vec{\varphi} \cdot (D_1\vec{\varphi} \times D_2\vec{\varphi})$ gives

$$Q^2 = \frac{1}{2}(D_i\vec{\varphi} \times D_j\vec{\varphi})^2. \quad (11)$$

The finite-energy requirement $\varepsilon(|\vec{x}| \rightarrow \infty) \rightarrow 0$ establishes the boundary conditions which must be satisfied by the fields of the model.

The total energy E is defined as the integral of the energy density (9), so that the implementation of the

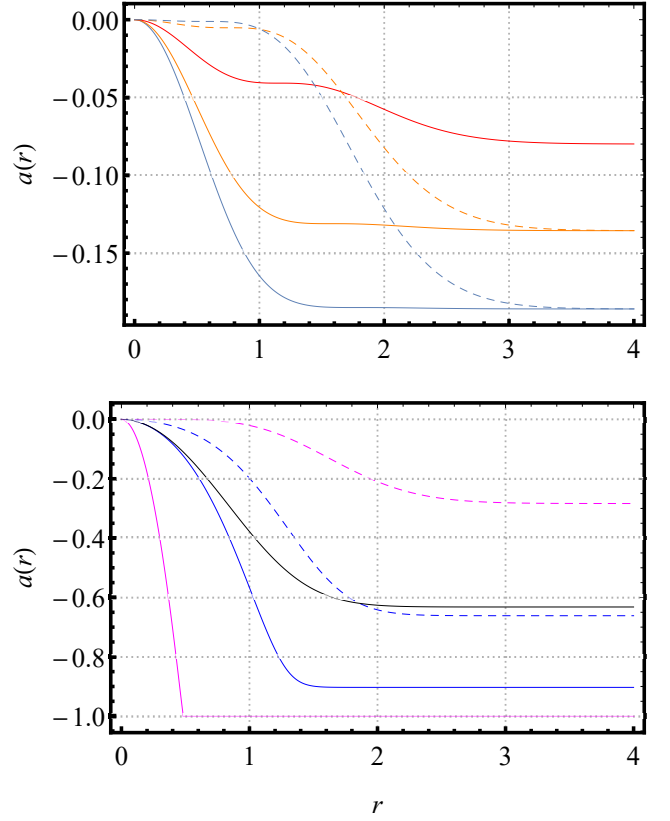


FIG. 2. Numerical solutions to the gauge profile function $a(r)$ obtained from Eqs. (45) and (46) for different values of α . Conventions as in the Fig. 1.

BPS formalism allows us to write

$$E = \int d^2\mathbf{x} \left[\frac{(GB \pm \lambda^2 g^2 \mathcal{W})^2}{2Gg^2} + \frac{\lambda^2}{2}(Q \pm Z)^2 \mp \lambda^2 B\mathcal{W} - \frac{\lambda^4 g^2}{2G} \mathcal{W}^2 \mp \lambda^2 QZ - \frac{\lambda^2}{2} Z^2 + V \right], \quad (12)$$

where we have introduced two auxiliary functions (to be determined later below), namely $\mathcal{W} \equiv \mathcal{W}(\varphi_n)$ and $Z \equiv Z(\varphi_n)$. Now, by using the expression

$$Q = \vec{\varphi} \cdot (\partial_1\vec{\varphi} \times \partial_2\vec{\varphi}) + \epsilon_{ij} A_i (\hat{n} \cdot \partial_j\vec{\varphi}) \quad (13)$$

together with $B = -\epsilon_{ij}\partial_i A_j$, we rewrite (12) as

$$E = \int d^2\mathbf{x} \left[\frac{(GB \pm \lambda^2 g^2 \mathcal{W})^2}{2Gg^2} + \frac{\lambda^2}{2}(Q \pm Z)^2 \mp \lambda^2 Z\vec{\varphi} \cdot (\partial_1\vec{\varphi} \times \partial_2\vec{\varphi}) \mp \lambda^2 \epsilon_{ij} [(\partial_j A_i)\mathcal{W} + A_i Z(\hat{n} \cdot \partial_j\vec{\varphi})] - \frac{\lambda^4 g^2}{2G} \mathcal{W}^2 - \frac{\lambda^2}{2} Z^2 + V \right]. \quad (14)$$

At this point, we transform the third row of Eq. (14) in

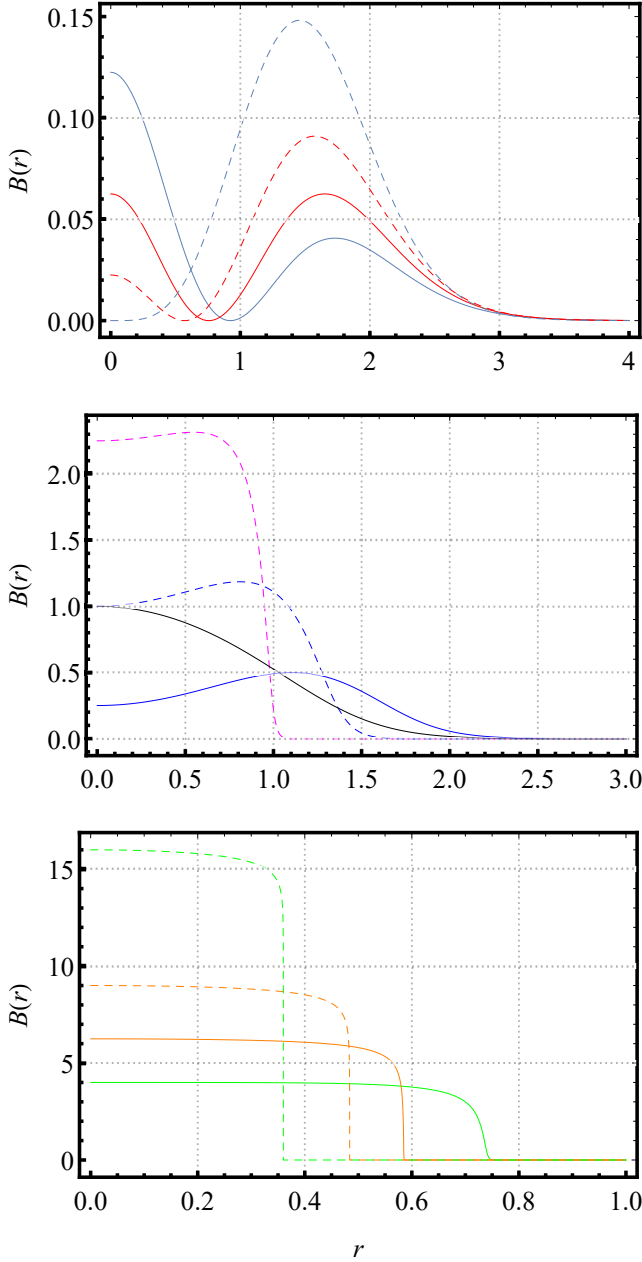


FIG. 3. Numerical solutions to the BPS magnetic field $B(r)$ obtained via Eqs. (45) and (46) for different values of α . Top: $\alpha = 0.65$ (solid nave line), $\alpha = 0.75$ (solid red line), $\alpha = 0.85$ (dashed red line) and $\alpha = 1$ (dashed nave line). Middle: $\alpha = 1.5$ (solid blue line), $\alpha = 2$ (dashed blue line) and $\alpha = 2.5$ (dashed magenta line). Bottom: $\alpha = 3$ (solid green line), $\alpha = 3.5$ (solid orange line), $\alpha = 4$ (dashed orange line) and $\alpha = 5$ (dashed green line). The usual profile is shown as a solid black line, for comparison.

a total derivative by choosing

$$Z = \frac{\partial \mathcal{W}}{\partial \varphi_n}, \quad (15)$$

such that

$$\partial_j \mathcal{W} = \frac{\partial \mathcal{W}}{\partial \varphi_n} (\hat{n} \cdot \partial_j \vec{\varphi}). \quad (16)$$

Next, we set the fourth row of Eq. (14) as being zero, from which we get the BPS potential $V(\varphi_n)$ as

$$V = \frac{\lambda^4 g^2}{2G} \mathcal{W}^2 + \frac{\lambda^2}{2} \left(\frac{\partial \mathcal{W}}{\partial \varphi_n} \right)^2. \quad (17)$$

Notably, $\mathcal{W}(\varphi_n)$ plays the role of a *superpotential* function which must be therefore constructed (or proposed) such that the self-dual potential $V(\varphi_n)$ becomes null when $\varphi_n \rightarrow 1$ (or $|\vec{x}| \rightarrow \infty$), in accordance with the Eq. (9). Consequently, the following boundary conditions must be satisfied,

$$\lim_{\varphi_n \rightarrow 1} \mathcal{W}(\varphi_n) = 0 \quad \text{and} \quad \lim_{\varphi_n \rightarrow 1} \frac{\partial \mathcal{W}}{\partial \varphi_n} = 0. \quad (18)$$

The total energy then becomes

$$E = \int d^2 \mathbf{x} \left[\frac{(GB \pm \lambda^2 g^2 \mathcal{W})^2}{2Gg^2} + \frac{\lambda^2}{2} \left(Q \pm \frac{\partial \mathcal{W}}{\partial \varphi_n} \right)^2 \mp \lambda^2 \left(\frac{\partial \mathcal{W}}{\partial \varphi_n} \right) \vec{\varphi} \cdot (\partial_1 \vec{\varphi} \times \partial_2 \vec{\varphi}) \mp \lambda^2 \epsilon_{ij} \partial_j (A_i \mathcal{W}) \right]. \quad (19)$$

In view of the boundary conditions (18), we observe that the contributions due to the total derivatives present in the second row of Eq. (19) vanish, from which we can express the total energy as

$$E = \bar{E} + E_{bps}, \quad (20)$$

where \bar{E} represents the integral composed by the quadratic terms, i.e.

$$\bar{E} = \int d^2 \mathbf{x} \left[\frac{(GB \pm \lambda^2 g^2 \mathcal{W})^2}{2Gg^2} + \frac{\lambda^2}{2} \left(Q \pm \frac{\partial \mathcal{W}}{\partial \varphi_n} \right)^2 \right], \quad (21)$$

and E_{bps} defines the energy lower bound, which reads

$$E_{bps} = \mp \lambda^2 \int d^2 \mathbf{x} \left(\frac{\partial \mathcal{W}}{\partial \varphi_n} \right) \vec{\varphi} \cdot (\partial_1 \vec{\varphi} \times \partial_2 \vec{\varphi}) > 0. \quad (22)$$

Here, we point out that the term $\vec{\varphi} \cdot (\partial_1 \vec{\varphi} \times \partial_2 \vec{\varphi})$ is related to the topological charge (or topological degree, also called winding number) of the Skyrme field by means of

$$\text{deg}[\vec{\varphi}] = -\frac{1}{4\pi} \int d^2 \mathbf{x} \vec{\varphi} \cdot (\partial_1 \vec{\varphi} \times \partial_2 \vec{\varphi}), \quad (23)$$

where $k \in \mathbb{Z} \setminus \{0\}$.

The total energy (20) satisfies the typical BPS inequality

$$E \geq E_{bps}, \quad (24)$$

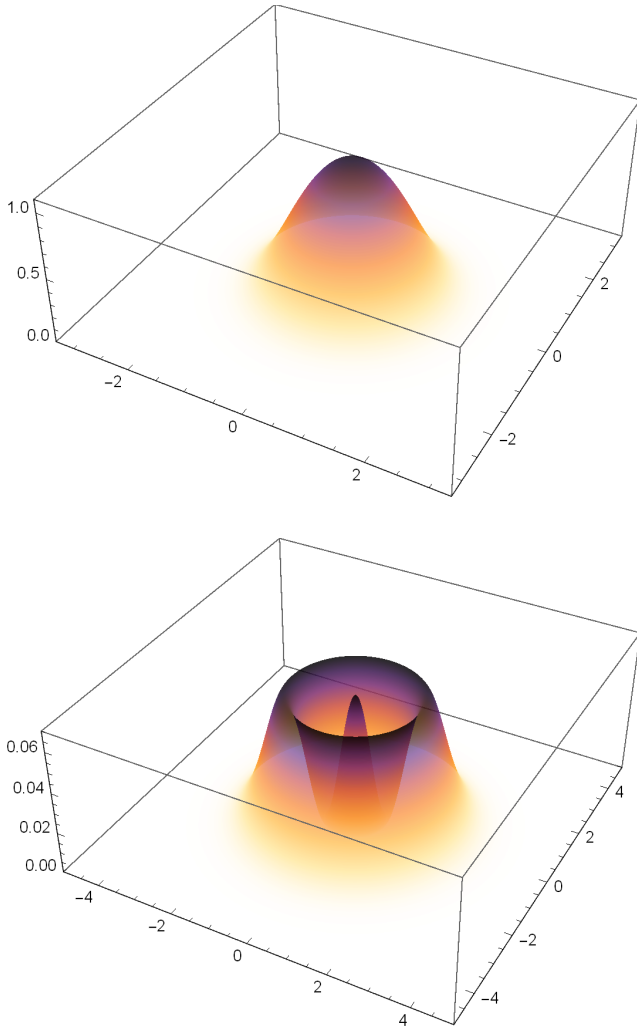


FIG. 4. Three-dimensional view of the solutions to $B(r)$. Top: usual profile. Bottom: solution for $\alpha = 0.75$.

because $\bar{E} \geq 0$. Then, the energy lower bound (the BPS one) is achieved when the fields give rise to configurations such that $\bar{E} = 0$, i.e. when the following set of first-order differential equations is satisfied:

$$GB = \mp g^2 \lambda^2 \mathcal{W}, \quad (25)$$

$$Q = \mp \frac{\partial \mathcal{W}}{\partial \varphi_n}. \quad (26)$$

Furthermore, from the combination between Eq. (10), the BPS equations above and the potential (17), one gets that the BPS energy density can be expressed as

$$\varepsilon_{bps} = \varepsilon_{bps}^M + \varepsilon_{bps}^S, \quad (27)$$

where we have defined

$$\varepsilon_{bps}^M = \frac{G}{g^2} B^2, \quad (28)$$

$$\varepsilon_{bps}^S = \lambda^2 Q^2, \quad (29)$$

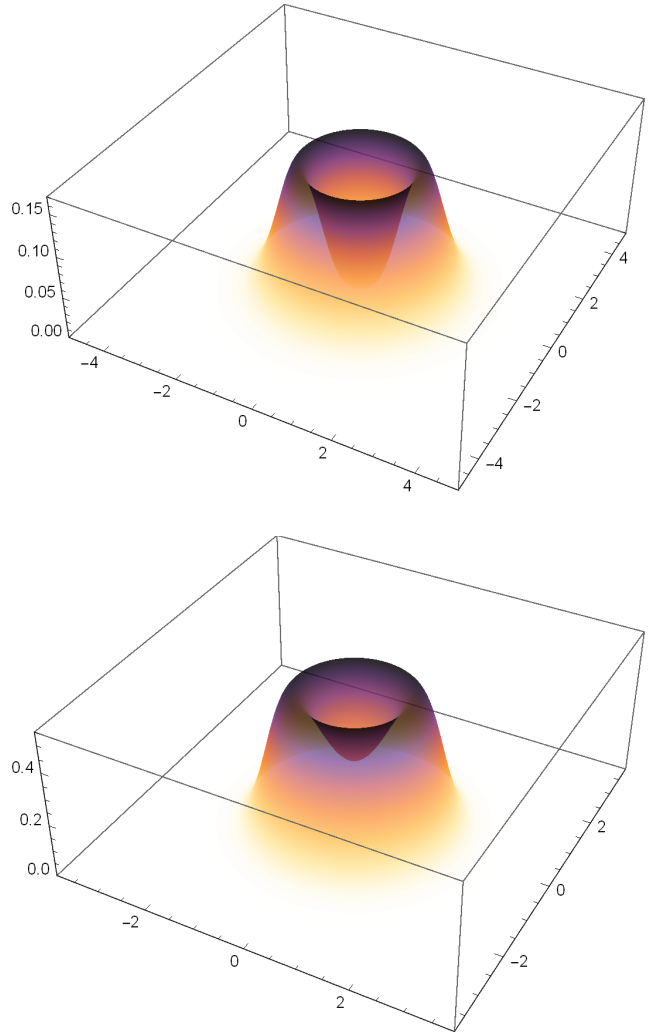


FIG. 5. Three-dimensional view of the solutions to $B(r)$. Top (bottom): solution for $\alpha = 1$ ($\alpha = 1.5$).

as the *magnetic energy density* and the *Skyrmion energy density*, respectively.

In what follows, we implement the radially symmetric ansatz. Without loss of generality, we set $\hat{n} = (0, 0, 1)$, from which we get $\varphi_n = \hat{n} \cdot \vec{\varphi} = \varphi_3$. In this case, the self-interacting potential $V = V(\varphi_3)$ allows the spontaneous breaking of the $SO(3)$ symmetry inherent to the Maxwell-Skyrme model (2), from which configurations with a nontrivial topology are expected to occur.

Moreover, in order to compare our results with the well-established ones, we study time-independent solutions with radial symmetry through the use of the standard ansatz, i.e.

$$A_i = -\epsilon_{ij} \hat{x}_j \frac{Na(r)}{r}, \quad (30)$$

$$\vec{\varphi} = \begin{pmatrix} \sin f \cos(N\theta) \\ \sin f \sin(N\theta) \\ \cos f \end{pmatrix}, \quad (31)$$

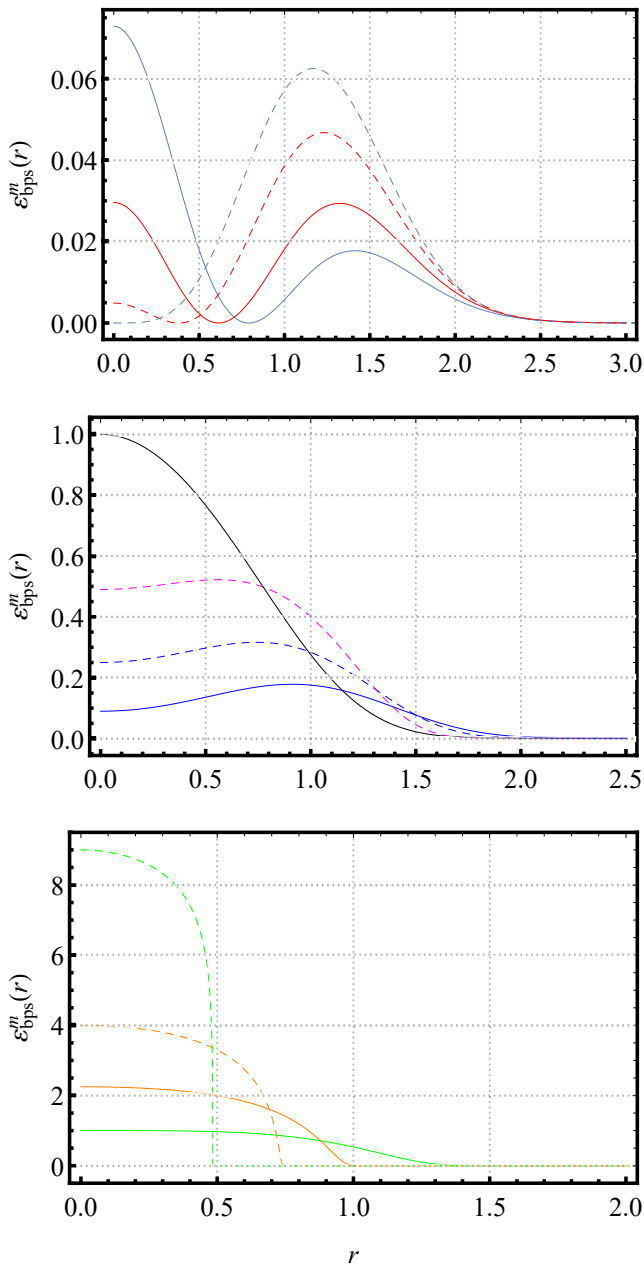


FIG. 6. Numerical solutions to the BPS magnetic energy density $\varepsilon_{bps}^M(r)$ obtained via Eqs. (45) and (46) for different values of α . Top: $\alpha = 0.73$ (solid blue line), $\alpha = 2(\sqrt{2} - 1)$ (solid red line), $\alpha = 0.93$ (dashed red line) and $\alpha = 1$ (dashed blue line). Middle: $\alpha = 1.3$ (solid blue line), $\alpha = 1.5$ (dashed blue line) and $\alpha = 1.7$ (dashed magenta line). Bottom: $\alpha = 2$ (solid green line), $\alpha = 2.5$ (solid orange line), $\alpha = 3$ (dashed orange line) and $\alpha = 4$ (dashed green line). The usual profile is shown as a solid black line, for comparison.

where r and θ are polar coordinates, ϵ_{ij} stands for the antisymmetric symbol (with $\epsilon_{12} = +1$) and $\hat{x}_i = (\cos\theta, \sin\theta)$ represents the unit vector. Also, N is the winding number of the Skyrme field, while the profile functions $f(r)$ and $a(r)$ are supposed to obey the boundary conditions which are known to support the existence

of regular solutions with finite energy, i.e.

$$f(r=0) = \pi \quad \text{and} \quad f(r \rightarrow \infty) \rightarrow 0, \quad (32)$$

$$a(r=0) = 0 \quad \text{and} \quad a'(r \rightarrow \infty) \rightarrow 0, \quad (33)$$

in which prime denotes the derivative with respect to the radial coordinate r .

The magnetic field in terms of the radially symmetric ansatz reads

$$B(r) = F_{21} = -\frac{N}{r} \frac{da}{dr}. \quad (34)$$

For convenience, it is useful to implement the field redefinition

$$h(r) = \frac{1}{2}(1 - \cos f), \quad (35)$$

which satisfy the following boundary conditions,

$$h(r=0) = 1 \quad \text{and} \quad h(r \rightarrow \infty) \rightarrow 0. \quad (36)$$

Consequently, both the magnetic permeability and the superpotential become functions of h only, i.e. $G \equiv G(h)$ and $\mathcal{W} \equiv \mathcal{W}(h)$, respectively. The boundary conditions satisfied by the superpotential can be summarised as

$$\lim_{r \rightarrow 0} \mathcal{W}(h) = \mathcal{W}_0, \quad \lim_{r \rightarrow \infty} \mathcal{W}(h) = 0, \quad \text{and} \quad \lim_{r \rightarrow \infty} \frac{\partial \mathcal{W}}{\partial h} = 0, \quad (37)$$

where $\mathcal{W}_0 = \mathcal{W}(h(r=0)) = \mathcal{W}(1)$, whereas the two last ones correspond to those which appear in Eq. (18).

Further, the magnetic energy density and the Skyrme energy density can be expressed in terms of the superpotential $\mathcal{W}(h)$ as

$$\varepsilon_{bps}^M = \lambda^4 g^2 \frac{\mathcal{W}^2}{G}, \quad (38)$$

$$\varepsilon_{bps}^S = \frac{\lambda^2}{4} \left(\frac{\partial \mathcal{W}}{\partial h} \right)^2, \quad (39)$$

respectively.

The BPS energy given by Eq. (22) can be calculated explicitly, its value reading

$$E_{bps} = \mp 2\pi \lambda^2 N \mathcal{W}_0, \quad (40)$$

i.e. a positive-definite quantity (considering $\mathcal{W}_0 > 0$). Here, the minus (plus) sign corresponds to $N < 0$ ($N > 0$).

The BPS equations (25) and (26) become

$$GB = \mp \lambda^2 g^2 \mathcal{W} \quad (41)$$

and

$$\frac{(1+a)}{r} \frac{dh}{dr} = \pm \frac{1}{4N} \frac{\partial \mathcal{W}}{\partial h}, \quad (42)$$

respectively. In summary, these equations describe a radially symmetric structure whose total energy is given by

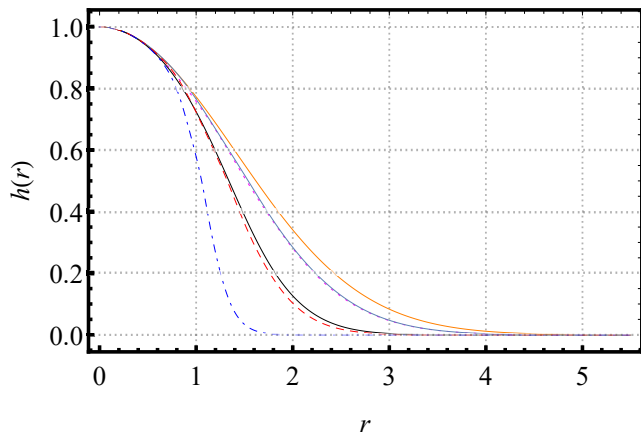


FIG. 7. Numerical solutions to the Skyrme profile function $h(r)$ obtained from the Eqs. (67) and (67) for $\alpha = 0$ (dotted magenta line), $\alpha = 0.5$ (solid orange line), $\alpha = 1$ (solid nave line), $\alpha = 1.5$ (dashed red line) and $\alpha = 2$ (dotdashed blue line). The usual solution appears as a solid black line, for comparison.

Eq. (40). Further, the BPS gauged skyrmions emerge as the numerical solutions of the first-order equations (41) and (42) obtained via the boundary conditions (33) and (36).

In the next Section, we demonstrate how the first-order framework introduced above can be used to generate legitimate BPS gauged skyrmions in the presence of a non-trivial magnetic permeability.

III. BPS SKYRMIONS IN MAGNETIC MEDIA

The first step to solve the BPS equations is the specification of the superpotential $\mathcal{W}(h)$. In the present manuscript, we use

$$\mathcal{W}(h) = \frac{h^2}{\lambda^2}, \quad (43)$$

where $\mathcal{W}_0 = \lambda^{-2}$, as desired. It is clear that the superpotential above satisfies the conditions given in the Eq. (37). The superpotential (43) is known to support skyrmions which attain their asymptotic values according to a Gaussian decay law, as explained recently in the Refs. [18–20].

The second step is to choose the function $G(h)$, i.e. the magnetic permeability. We look for gauged skyrmions which behave standardly at the boundaries and have a noncanonical profile for intermediate values of the radial coordinate r . This type of configuration was recently investigated by some of us in the context of an extended Maxwell- $CP(2)$ system, see the Ref. [26], for instance. Then, for the present analysis, we select two different magnetic media, as shown below.

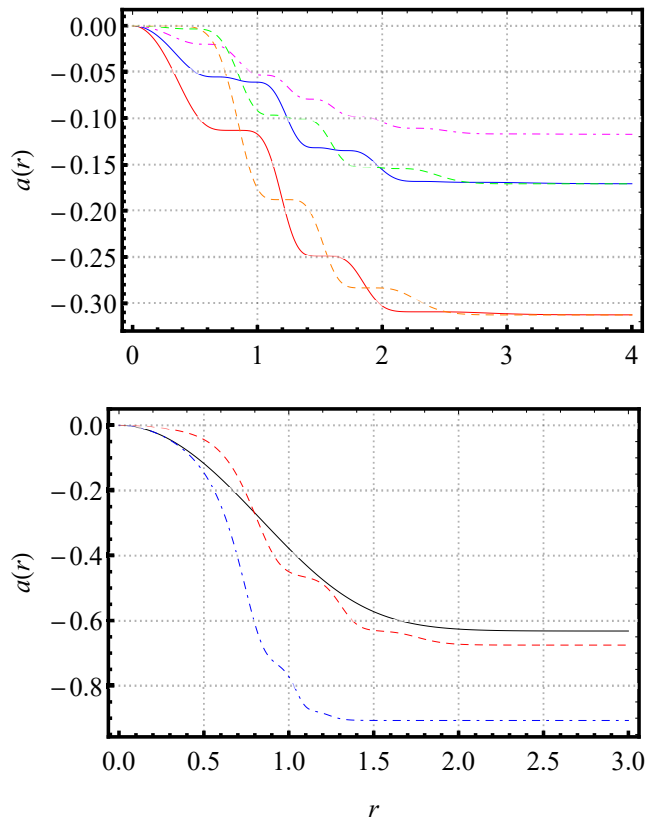


FIG. 8. Numerical solutions to the gauge profile function $a(r)$ obtained from Eqs. (67) and (68) for different values of α . Top: $\alpha = 0$ (solid red line), $\alpha = 0.25$ (solid blue line), $\alpha = 0.50$ (dotdashed magenta line), $\alpha = 0.75$ (dashed green line) and $\alpha = 1$ (dashed orange line). Bottom: $\alpha = 1, 5$ (dashed red line), $\alpha = 2$ (dotdashed blue line) and the usual profile (solid black line).

A. First model

In order to generate the aforementioned profiles, we choose the magnetic permeability $G(h)$ as

$$G(h) = \frac{1}{(\alpha - h^2)^\beta}, \quad (44)$$

where α and β are positive integer numbers. In particular, we intend to clarify how the parameter α changes the shape of the magnetic field along the radial coordinate, from which we set $\beta = 2$. For the sake of simplicity, we also choose the values $g = \lambda = 1$ and $N = 1$ (i.e. the lower signs in the BPS equations).

In view of the choices above, the BPS equations (41) and (42) reduce to

$$\frac{1}{r} \frac{da}{dr} = -h^2 (\alpha - h^2)^2, \quad (45)$$

$$\frac{(1+a)}{r} \frac{dh}{dr} = -\frac{1}{2}h, \quad (46)$$

which we solve numerically via the implementation of a

finite-difference scheme together with the boundary conditions (33) and (36).

In this sense, the figures 1 and 2 show respectively the numerical profiles to $h(r)$ and $a(r)$ for different values of α . In general, this parameter controls the distance over which those fields effectively spread, therefore affecting the intensity of the interaction between these configurations. Here, it is also important to note that the solutions to the gauge profile function $a(r)$ with $\alpha < 1$ are characterized by the presence of interesting plateaus which appear for intermediate values of the radial coordinate r . For $\alpha > 3$, both fields assume a compact-like profile for increasing α . Such a behavior is analogue to that already found in the standard case ($G = 1$) for increasing values of the coupling constant g .

As we explain below, these structures give rise to the formation of nonstandard internal structures which distinguish the behavior of the corresponding magnetic field, see the analytical considerations in the sequence.

1. The magnetic field

In the Fig. 3, we show the numerical solutions to the magnetic field $B(r)$, from which it is possible to see how the shape of this field depends on the value of α in a dramatic way. We now proceed with an analytical study of such a dependence.

In order to describe the way the parameter α affects the shape of the magnetic sector, we write the magnetic field

$$B(r) = h^2 (\alpha - h^2)^2, \quad (47)$$

whose first derivative provides

$$\frac{d}{dr}B = 2h (\alpha - h^2) (\alpha - 3h^2) \frac{dh}{dr}. \quad (48)$$

Now, given that the solution to the Skyrme profile function $h(r)$ varies monotonically from 1 (at $r = 0$) to 0 (in the limit $r \rightarrow \infty$, i.e. the first derivative of the $h(r)$ is always negative), one gets that the condition $B'(R) = 0$ provides the extreme points R of interest (the ones located away from the origin)

$$h(R_1) = h_1 = \sqrt{\alpha} < 1, \quad (49)$$

$$h(R_2) = h_2 = \sqrt{\frac{\alpha}{3}} < 1, \quad (50)$$

where $0 < R_1 < R_2$.

At these points, the magnetic field reads

$$B_1 = B(h_1) = 0, \quad (51)$$

$$B_2 = B(h_2) = \frac{4}{27}\alpha^3, \quad (52)$$

respectively. The first value, B_1 , becomes a local minimum if $\alpha < 1$, whereas B_2 results in a local maximum

if $\alpha < 3$. Moreover, from Eq. (47), the value of the magnetic field at the origin is given by

$$B_0 = B(r = 0) = (\alpha - 1)^2. \quad (53)$$

In view of the Eqs. (51), (52) and (53) above, we enumerate six different pictures to be considered based on the values of α . In this case, it is important to emphasize that we are considering all the values of r , except the ones located in the asymptotic region $r \rightarrow \infty$.

a. The first picture: It is defined for $\alpha = 0$, from which one gets that the first-order equations (45) and (46) can be rewritten as

$$\frac{1}{r} \frac{da}{dr} = -h^6, \quad (54)$$

$$\frac{(1+a)}{r} \frac{dh}{dr} = -\frac{1}{2}h, \quad (55)$$

which, after the field redefinition $H(r) = [h(r)]^3$, reads

$$\frac{1}{r} \frac{dH}{dr} = -H^2, \quad (56)$$

$$\frac{(1+a)}{r} \frac{dH}{dr} = -\frac{3}{2}H. \quad (57)$$

In this case, despite the redefinition applied on the Skyrme profile function, we note that the resulting first-order Eqs. (56) and (57) can be obtained directly from the general ones (41) and (42) for $G = 1$, $g = N = 1$, $\sigma = 2$ and $\lambda = \sqrt{1/3}$. We then conclude that the a priori nontrivial case defined by $G(h) = h^{-4}$ stands for a merely redefinition of the usual case (defined by $G = 1$) with a different value of the coupling constant λ . As a consequence, we do not expect significant changes to occur on the shape of the solutions, especially on that of the magnetic sector. Therefore, in what follows, we consider only the case with nonvanishing values of α .

b. The second picture: It occurs when $0 < \alpha < 1$. In this context, the solution (49) is satisfied at some point $r = R_1$ (defined via $h(r = R_1) = h_1 = \sqrt{\alpha}$). At this point, the magnetic field vanishes (i.e., $B(r = R_1) = 0$, see Eq. (51)), from which it is reasonable to infer that the magnetic solution describes a centered lump surrounded by a ring: the lump is positioned at the origin, its amplitude being given by Eq. (53) itself, while the radius of the ring is located at some point $r = R_2 > R_1$ (defined by $h(r = R_2) = h_2 = \sqrt{\alpha/3}$, see Eq. (50)), the amplitude of the ring standing for $B(r = R_2) = (4/27)\alpha^3$, according to the previous Eq. (52).

We highlight how α determines the difference between the amplitudes of these two amplitudes: for $0 < \alpha < 0.75$, the magnitude of the centered lump is taller than that of the ring (i.e. $(\alpha - 1)^2 > (4/27)\alpha^3$). On the other hand, when $\alpha = 0.75$, the two magnitudes have the very same amplitude. Finally, for $0.75 < \alpha < 1$, the magnitude of the ring is taller than that of the lump positioned at $r = 0$ (i.e. $(\alpha - 1)^2 < (4/27)\alpha^3$).

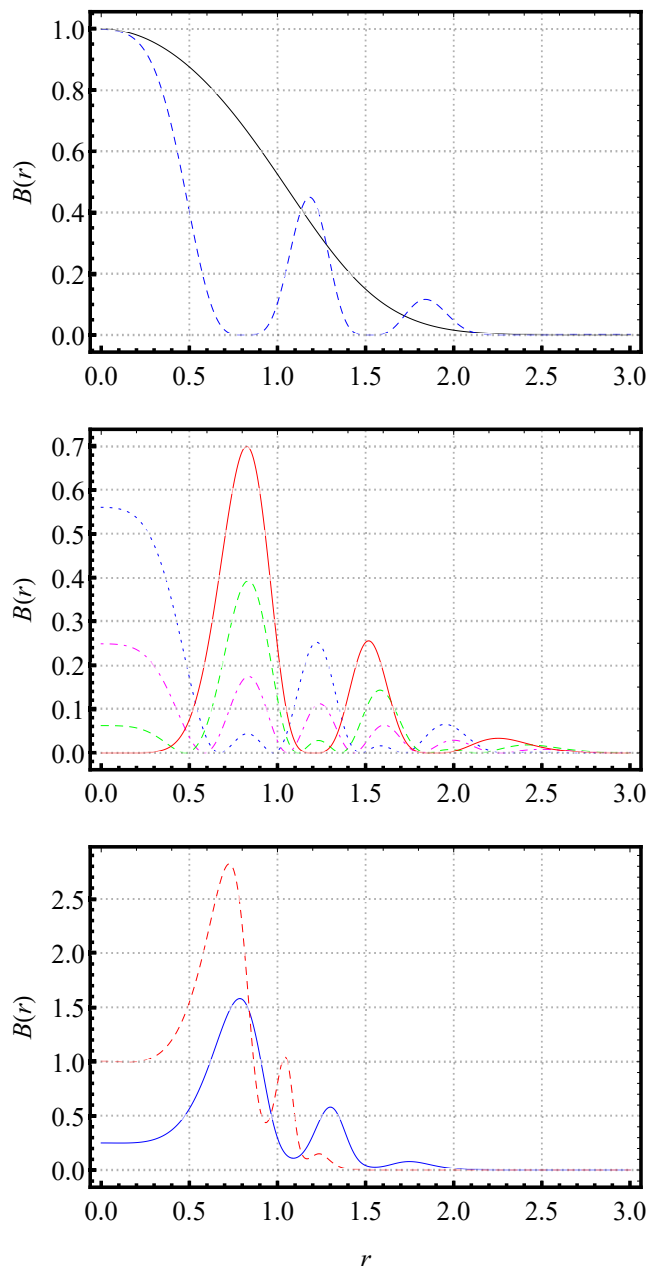


FIG. 9. Numerical solutions to the BPS magnetic field $B(r)$ obtained via Eqs. (67) and (68) for different values of α . Top: $\alpha = 0$ (dashed blue line) and the usual profile (solid black line). Middle: $\alpha = 0.25$ (dotted blue line), $\alpha = 0.50$ (dotdashed magenta line), $\alpha = 0.75$ (dashed green line) and $\alpha = 1$ (solid red line). Bottom: $\alpha = 1.5$ (solid blue line) and $\alpha = 2$ (dashed red line).

The parameter α also controls the values of both R_1 (i.e. the point at which $B(r)$ vanishes) and R_2 (the radius of the ring): as α increases, the values of $h_1 = \sqrt{\alpha}$ and $h_2 = \sqrt{\alpha/3}$ also increase and, once $h(r)$ varies monotonically from 1 to 0, both R_1 and R_2 decrease (i.e. move toward the origin).

c. The third picture: The case with $\alpha = 1$ defines the third picture, for which Eq. (49) holds at the origin only, i.e. $h(r=0) = h_1 = 1$, which agrees with the boundary condition (36). Therefore, the magnetic field vanishes at $r = 0$, which agrees with the result which comes from Eq. (53) for $\alpha = 1$. We then conclude that the resulting magnetic profile stands for a single ring whose radius is located at some point $r = R_2$ (defined by $h(r = R_2) = h_2 = \sqrt{1/3}$, see the Eq. (50)), its magnitude being equal to $B(r = R_2) = 4/27$, see the Eq. (52).

d. The fourth picture: It is defined for $1 < \alpha < 3$. In this case, Eq. (49) is not satisfied at all, from which one gets that $B(r)$ does not vanish for intermediate values of r (i.e. Eq. (51) does not hold anymore). The magnetic solution therefore stands for a volcano centered at the origin: the value of the $B(r)$ at $r = 0$ is still given by Eq. (53), while its global maximum is reached at $r = R_2$ (such that $h(r = R_2) = h_2 = \sqrt{\alpha/3}$, for which the magnetic profile attains the value given by Eq. (52)). The volcano is therefore completely characterized by the fact that $B(r = R_2) > B(r = 0)$. Moreover, α also controls the value of R_2 : when α increases, the value of $h(r = R_2) = \sqrt{\alpha/3}$ also increases and, once that $h(r)$ varies monotonically from 1 (at $r = 0$) to 0 (in the limit $r \rightarrow \infty$), the value of R_2 decreases.

e. The fifth picture: We continue our study and define the fifth picture for $\alpha = 3$, which leads us to the conclusion that Eq. (49) is again not satisfied at all (i.e. $B(r)$ does not vanish for intermediate r). On the other hand, Eq. (50) is satisfied only at the origin (i.e. $h(r=0) = h_2 = 1$, which agrees with the condition (36)). At this point, the Eq. (52) reveals that the magnetic field is equal to $B(h = h_2) = 4$, which coincides with the result which arises from Eq. (53). As a consequence, the magnetic sector describes a compact-like structure centered at $r = 0$.

f. The sixth picture: Finally, for $\alpha > 3$, both Eqs. (49) and (50) are not satisfied. In such a scenario, one notes that the magnetic field has no valleys and no additional peaks, i.e. $B(r)$ varies monotonically from $B(r=0) = (\alpha - 1)^2$ to $B(r \rightarrow \infty) \rightarrow 0$ (a localized magnetic flux, as expected). As a result, as α increases, the magnetic field develops a more and more compact-like profile centered at $r = 0$. As explained previously, such a behavior is analogue to that already found in the standard case (with $G = 1$) for increasing values of the electromagnetic coupling constant g .

2. The BPS energy density

We now focus our attention on the energy density of the resulting BPS configurations and investigate how this profile is affected by the values of α . Moreover, in view of our choices (43) and (44) for $\mathcal{W}(h)$ and $G(h)$, we get

TABLE I. Results for $\alpha = 0.25$. The exact roots of Eq. (71) (first column), the approximate roots of Eq. (72) (second column) and the values of $B(r)$ calculated at these last roots (third column). The magnetic field at the origin is given by $B_0 = 0.5625$. The approximate results are given with an accuracy of 10^{-4} .

Roots of (71)	Roots of (72)	Values of $B(r)$
8/9	0.8350	0.0435
7/9	0.6729	0.2524
5/9	0.5028	0.0157
4/9	0.3454	0.0648
2/9	0.1746	0.0018
1/9	0.0577	0.0008

that ε_{bps}^M and ε_{bps}^S can be rewritten in the form

$$\varepsilon_{bps}^M = h^4 (\alpha - h^2)^2, \quad (58)$$

$$\varepsilon_{bps}^S = h^2, \quad (59)$$

where we have already implemented $g = \lambda = 1$ and $\beta = 2$ (i.e. the choices inherent to the theoretical scenario which we are effectively investigating in this manuscript).

Here, given that the Skyrmion profile $h(r)$ is constrained to satisfy the boundary conditions (36) monotonically, it is possible to infer that the numerical profile for $\varepsilon_{bps}^S = h^2$ (which does not depend on α explicitly) stands for a lump centered at $r = 0$ for all values of α , from which we conclude that there is no novelty to be discussed concerning this solution.

On the other hand, the solution for the magnetic energy density $\varepsilon_{bps}^M = h^4 (\alpha - h^2)^2$ depends on α explicitly. It is therefore possible to study the effects caused by different values of α on the shape of the solution for ε_{bps}^M by following the same route as it was done for the magnetic sector. In this sense, we calculate

$$\frac{d}{dr} \varepsilon_{bps}^M = 4h^3 (\alpha - h^2) (\alpha - 2h^2) \frac{dh}{dr}, \quad (60)$$

which provides the extreme values (here, $0 < R_3 < R_4$)

$$h(R_3) = h_3 = \sqrt{\alpha} < 1, \quad (61)$$

$$h(R_4) = h_4 = \sqrt{\frac{\alpha}{2}} < 1, \quad (62)$$

via which one gets the corresponding values of ε_{bps}^M as

$$\varepsilon_{bps,3}^M = \varepsilon_{bps}^M(h_3) = 0, \quad (63)$$

$$\varepsilon_{bps,4}^M = \varepsilon_{bps}^M(h_4) = \frac{\alpha^4}{16}, \quad (64)$$

while the value of such density at the origin can be obtained directly from Eq. (58), i.e.

$$\varepsilon_{bps,0}^M = \varepsilon_{bps}^M(r=0) = (\alpha - 1)^2, \quad (65)$$

where we have used $h(r=0) = 1$.

As it was done during the study of the magnetic profile, we again organize our analysis based on the values of α , from which it is possible to define six different pictures to be investigated.

a. The first picture: As we have explained before, it is defined by $\alpha = 0$ and can be interpreted as a redefinition of the usual case with a different value of λ , from which we conclude that this case is not that interesting. Therefore, in what follows, we consider only those cases with nonvanishing values of the parameter α .

b. The second picture: As before, it comes through $0 < \alpha < 1$, from which one gets that Eq. (61) is satisfied at the point $r = R_3$ (i.e. $h(r=R_3) = h_3 = \sqrt{\alpha}$). At this position, the magnetic energy density vanishes (i.e. $\varepsilon_{bps}^M(r=R_3) = 0$, see Eq. (63)), from which we infer that the resulting profile stands for a lump (positioned at $r = 0$, its amplitude being equal to $\varepsilon_{bps}^M(r=0) = (\alpha - 1)^2$, see the Eq. (65)) surrounded by a ring (whose radius is defined at $r = R_4 > R_3$, with R_4 defined by $h(r=R_4) = h_4 = \sqrt{\alpha/2}$, see Eq. (62)), its amplitude being given by $\varepsilon_{bps}^M(r=R_4) = \alpha^4/16$, see Eq. (64).

We point out that α modulates the difference between the magnitudes of these two amplitudes, i.e. when $0 < \alpha < 2(\sqrt{2} - 1)$, the peak of the lump at $r = 0$ is taller than that of the ring at $r = R_4$ (i.e. $(\alpha - 1)^2 > \alpha^4/16$). In addition, the two peaks have the very same magnitude for $\alpha = 2(\sqrt{2} - 1)$. However, when $2(\sqrt{2} - 1) < \alpha < 1$, the peak of the ring at $r = R_4$ is taller than that located at the origin (i.e. $(\alpha - 1)^2 < \alpha^4/16$).

It is clear that $R_1 = R_3$ [note that Eq. (49) is exactly the Eq. (61)], from which we get that the magnetic field and the magnetic energy density inevitably vanish at the very same point, see Eqs. (47) and (58), respectively. Moreover, still as a consequence of $R_1 = R_3$, we conclude that α controls the position of the valley between the two peaks of the magnetic energy in very same way as it determines the location of the valley between the two peaks of the magnetic field itself, see the previous discussion.

The parameter α controls not only the value of R_3 , but also that of R_4 (i.e. the radius of the ring): when α increases, the value of $h(r=R_4) = h_4 = \sqrt{\alpha/2}$ increases and, therefore, R_4 itself decreases.

TABLE II. Results for $\alpha = 0.50$. Conventions as in the Table I. The magnetic field at the origin is given by $B_0 = 0.25$. The approximate results are given with an accuracy of 10^{-4} .

Roots of (71)	Roots of (72)	Values of $B(r)$
11/12	0.8367	0.1743
9/12	0.6709	0.1118
7/12	0.5055	0.0632
5/12	0.3415	0.0285
3/12	0.1817	0.0076
1/12	0.0456	0.0002

TABLE III. Results for $\alpha = 0.75$. Conventions as in the Table I. The magnetic field at the origin is given by $B_0 = 0.0625$. Accuracy of 10^{-4} .

Roots of (71)	Roots of (72)	Values of $B(r)$
17/18	0.8384	0.3930
13/18	0.6688	0.0279
11/18	0.5083	0.1430
7/18	0.3375	0.0070
5/18	0.1884	0.0178
1/18	0.0314	3×10^{-5}

c. The third picture: It is again characterized by $\alpha = 1$. In this case, Eq. (61) is satisfied only at the origin (note that this result agrees with Eq. (36)). At this point, the magnetic energy density vanishes, from which we conclude that the corresponding profile stands for a single ring whose global maximum is located at $r = R_4$ (with R_4 defined by $h(r = R_4) = h_4 = \sqrt{1/2}$, see Eq. (62)), the maximum itself being given by $\varepsilon_{bps}^M(r = R_4) = 1/16$, see Eq. (64).

d. The fourth picture: It is defined by the values of α within the range $1 < \alpha < 2$. In such a scenario, Eq. (61) is not satisfied, from which one gets that the magnetic energy does not vanish for intermediate values of r . As a consequence, the solution for $\varepsilon_{bps}^M(r)$ results develops a volcano profile centered at the origin: the value of that function at $r = 0$ is given by the previous Eq. (65), with the global maximum being located at $r = R_4$ (such that $h(r = R_4) = h_4 = \sqrt{\alpha/2}$). At this point, the magnetic energy density reaches the value $\varepsilon_{bps}^M(r = R_4) = \alpha^4/16$, see Eq. (64). The volcano is then characterized by the fact that $\varepsilon_{bps}^M(r = R_4) > \varepsilon_{bps}^M(r = 0)$.

The parameter α also controls the value of R_4 itself, i.e. when α increases, the value of $h(r = R_4) = \sqrt{\alpha/2}$ increases, while R_4 moves toward $r = 0$.

e. The fifth picture: It is defined by $\alpha = 2$. Again, Eq. (61) does not hold anymore (i.e. $\varepsilon_{bps}^M(r)$ does not vanish for intermediate r). Moreover, Eq. (62) is satisfied only at $r = 0$, where the magnetic energy is equal to the unity (this result coincides with the one which comes from Eq. (65) for $\alpha = 2$). We then conclude that the magnetic energy profile stands for a lump with a compact profile centered at the origin.

f. The sixth picture: We end our analysis by considering the picture defined for $\alpha > 2$, for which none of Eqs. (61) and (62) is satisfied. This fact reveals that the solution for $\varepsilon_{bps}^M(r)$ varies monotonically (i.e. with no valleys and no additional peaks) from $\varepsilon_{bps}^M(r = 0) = (\alpha - 1)^2$ to $\varepsilon_{bps}^M(r \rightarrow \infty) \rightarrow 0$. As a consequence, the resulting configuration (i.e. a lump) develops a more and more compact-like profile centered at $r = 0$ whenever α increases. A similar situation happens for increasing values of g in the standard case ($G = 1$).

B. Second model

The previous idea about gauged skyrmions with internal structures can be generalized to include a BPS magnetic configuration with multiple zeros. In order to illustrate this possibility, we choose the magnetic permeability as

$$G(h) = \frac{1}{[\alpha - \cos^2(n\pi h)]^\beta}, \quad (66)$$

where both α and β are again positive integer numbers.

Eq. (66) reveals that, given a particular value of α such that $0 \leq \alpha \leq 1$, the integer parameter n counts the number of singularities which characterize the function $G(h)$ and therefore it is expected to define also the number of zeros in the resulting magnetic solution. It is important to highlight that a magnetic BPS soliton with multiple zeros was recently found by Bazeia et al. in the context of an enlarged Maxwell-Higgs theory [27] and that such a profile can be used as an attempt to explain the behaviour of radially symmetric configurations at the nanometric scale.

In view of Eq. (66), we focus our attention on the effects which the values of α promote on the shape of the resulting solutions, so we set $\beta = 2$ and $n = 3$. Furthermore, as previously, we fix $g = \lambda = 1$ and $N = 1$, from which we get that the first-order equations (41) and (42) assume the form

$$\frac{1}{r} \frac{da}{dr} = -h^2 [\alpha - \cos^2(3\pi h)]^2, \quad (67)$$

$$\frac{(1+a)}{r} \frac{dh}{dr} = -\frac{1}{2}h, \quad (68)$$

which must be solved by means of the usual finite-difference scheme according to the conditions (33) and (36).

The figures 7, 8, 9 and 12 show the numerical results obtained for different values of α . As before, in all these figures, the standard profile (i.e. the one for $G = 1$) is depicted as a solid black line, for comparison.

In particular, the figures 7 and 8 present the solutions to $h(r)$ and $a(r)$, respectively, from which we see that, as in the case studied previously, different values of α in general change the length over which the cores of $h(r)$ and $a(r)$ spread. It is also interesting to note the formation of multiple plateaus in the solutions for the gauge profile function $a(r)$: as the reader can infer (based on the case investigated above), these plateaus indicate the existence of a magnetic field characterized by an internal structure with multiple zeros (which we again explain theoretically based on the values of α below).

1. The magnetic field

The Figure 9 depicts the profiles to the magnetic field $B(r)$, from which the reader can verify how the shape

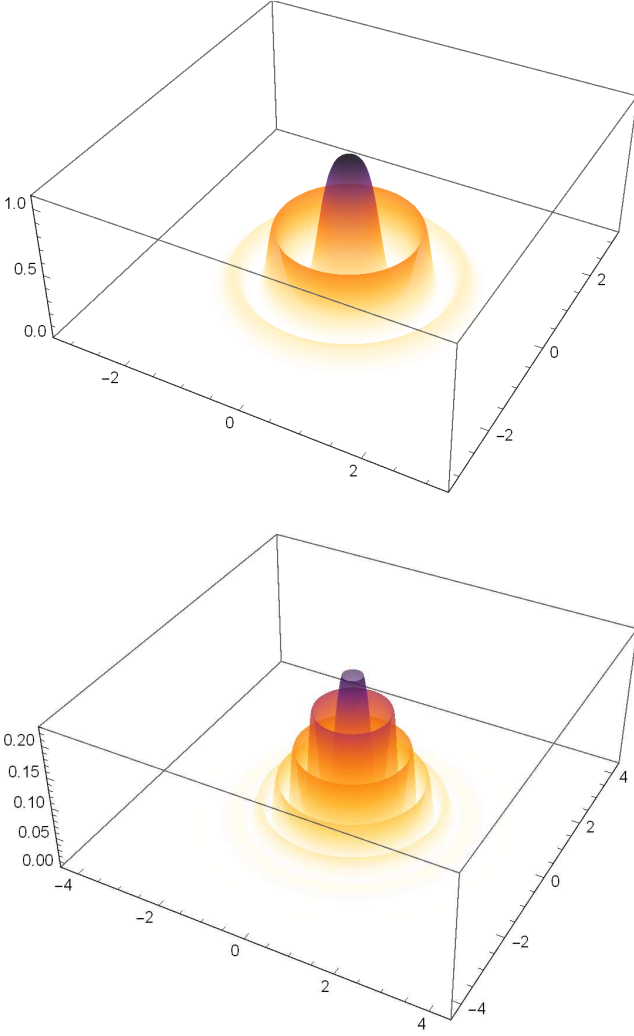


FIG. 10. Three-dimensional view of the solutions to $B(r)$. Top (bottom): solution for $\alpha = 0$ ($\alpha = 0.5$).

of this field changes dramatically as α itself varies. As before, we now proceed with an analytical investigation on such a relationship, the starting-point being the radially symmetric expression for the effective first-order BPS magnetic field, i.e.

$$B = h^2 [\alpha - \cos^2(3\pi h)]^2, \quad (69)$$

which was obtained through the combination between the equations (41), (43) and (66) and the conventions which we have adopted in this manuscript regarding the parameters of the model.

From Eq. (69), we obtain

$$\begin{aligned} \frac{d}{dr} B &= 2h [\alpha - \cos^2(3\pi h)] \\ &\times \left[[6\pi h \sin(3\pi h) - \cos(3\pi h)] \cos(3\pi h) + \alpha \right] \frac{dh}{dr} \end{aligned} \quad (70)$$

from which one gets that $B'(r) = 0$ gives rise to ($h(r)$ is constrained to vary from 1 to 0 monotonically)

$$\cos^2(3\pi h) = \alpha, \quad (71)$$

$$[6\pi h \sin(3\pi h) - \cos(3\pi h)] \cos(3\pi h) = -\alpha, \quad (72)$$

where, as before, we are considering all the values of r , except those ones in $r \rightarrow \infty$.

In addition, the value of $B(r)$ at the origin can be obtained from Eq. (69), i.e.

$$B_0 = (\alpha - 1)^2, \quad (73)$$

where we have again used the definition $B_0 = B(r = 0)$.

The reader is expected to infer that from this point on the analysis follows the same route already stated during the investigation of the previous case, i.e. for a particular value of α , Eqs. (71) and (72) must be solved for the values of h_i . In the sequence, the magnetic field (69) for that particular α must be evaluated at those different h_i 's and its resulting values must be classified as local maxima or minima (including zero) of the corresponding solution. Based on this classification, it must be possible to label the magnetic solution as a lump or as a ring and also to describe theoretically how its main dimensions (such as amplitude and radius) depend on the value of α .

Once that we have explained how to proceed, below we use such a prescription to study some ranges of values for α in order to illustrate our results.

a. The case $\alpha = 0$: In this case, Eq. (71) can be reduced to

$$\cos(3\pi h) = 0, \quad (74)$$

whose exact roots can be easily verified to be

$$h(\mathcal{R}_1) = h_1 = \frac{5}{6}, \quad (75)$$

$$h(\mathcal{R}_3) = h_3 = \frac{3}{6}, \quad (76)$$

$$h(\mathcal{R}_5) = h_5 = \frac{1}{6}, \quad (77)$$

from which one calculates $B_1 = B_2 = B_3 = 0$ (with $B_i = B(h = h_i)$), i.e. the points above represent 3 (three) different zeros of the magnetic field.

On the other hand, for $\alpha = 0$, Eq. (72) can be written as

$$[6\pi h \sin(3\pi h) - \cos(3\pi h)] \cos(3\pi h) = 0, \quad (78)$$

which promptly gives

$$\cos(3\pi h) = 0, \quad (79)$$

$$6\pi h \sin(3\pi h) - \cos(3\pi h) = 0. \quad (80)$$

The equation (79) is the same Eq. (74), from which we get that Eq. (78) is satisfied by the values of h given

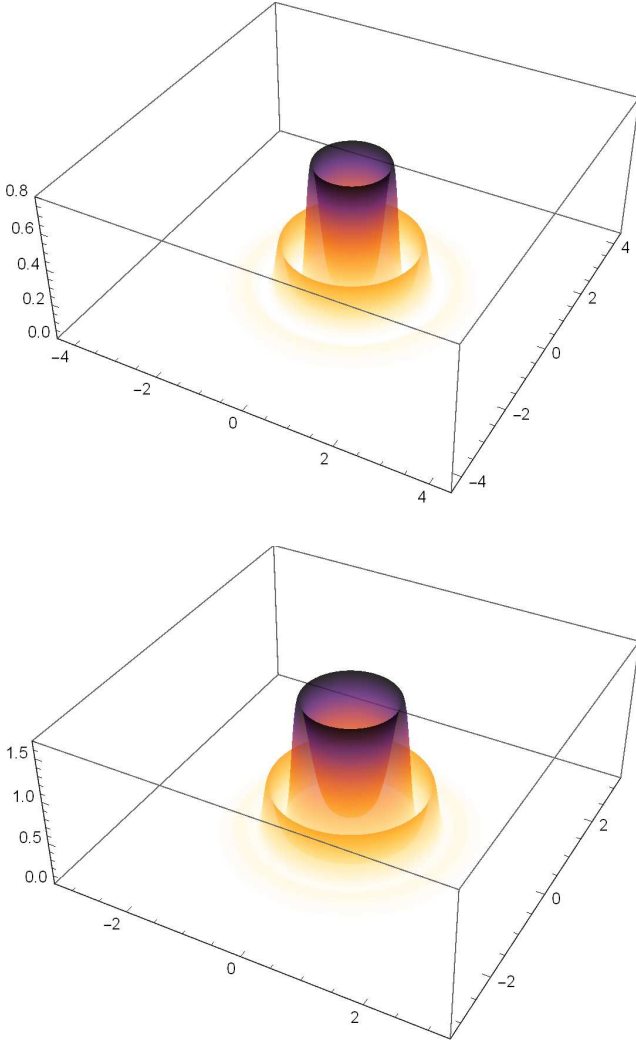


FIG. 11. Three-dimensional view of the solutions to $B(r)$. Top (bottom): solution for $\alpha = 1$ ($\alpha = 1.5$).

by Eqs. (77), (76) and (75) for which $B(r)$ vanishes, see the discussion therein.

In addition, Eq. (80) stands for a transcendental one whose roots must be therefore evaluated numerically. In this context, there are three different solutions, i.e.

$$h_2(r = \mathcal{R}_2) \approx 0.6750 \quad (B_2 \approx 0.4500), \quad (81)$$

$$h_4(r = \mathcal{R}_4) \approx 0.3493 \quad (B_4 \approx 0.1166), \quad (82)$$

$$h_6(r = \mathcal{R}_6) \approx 0.0693 \quad (B_6 \approx 0.0019), \quad (83)$$

via which we get that the corresponding values of $B(r)$ stand for the local maxima when $\alpha = 0$.

Moreover, the value of the magnetic field at the origin is given by

$$B_0 = 1, \quad (84)$$

according to the previous Eq. (73).

The results calculated above reveal that the corresponding magnetic profile presents a global maximum at

$r = 0$ and a much more sophisticated internal structure which interpolates between three different zeros [whose locations are defined by Eqs. (75), (76) and (77)] and the three different local maxima (with the respective localisations) given by Eqs. (81), (82) and (83), before finally vanishing in the asymptotic limit, the resulting profile therefore standing for a centered lump surrounded by three concentric rings.

b. For $0 < \alpha < 1$: In this case, Eq. (71) predicts the existence of 6 (six) different roots whose exact values can be calculated directly from

$$h_{i,\pm}(r = \mathcal{R}_{i,\pm}) = \frac{\arccos(\pm\sqrt{\alpha})}{3\pi} + \frac{(i-1)}{3}, \quad (85)$$

where $i = 1, 2$ and 3 .

At these six points, the magnetic field vanishes identically, from which one gets that, for a particular value of α such that $0 < \alpha < 1$, $B(r)$ presents 6 (six) different zeros.

In addition, Eq. (72) again does not support an exact solution and therefore must be solved numerically for different values of α within the range $0 < \alpha < 1$. The approximate roots obtained this way eventually define the peaks inherent to the internal structure which characterizes the magnetic solution. As before, the value of $B(r)$ at $r = 0$ is still given by Eq. (73).

We illustrate our analysis by plotting the solutions for the values $\alpha = 0.25$, $\alpha = 0.50$ and $\alpha = 0.75$, from which we summarize the corresponding results in the tables I, II and III below, respectively. In these tables, the values of $h_{i,\pm}$ (which appear in the first column) stand for the exact roots of Eq. (71) (i.e. the points at which the magnetic field vanishes), while the values of h_j (displayed on the second column) are the approximate roots of the transcendental Eq. (72). Finally, the third column shows the values of $B(r)$ calculated at these various h_j , i.e. $B_j = B(h = h_j)$ (the peaks of the magnetic profile). In view of these results, we conclude that the resulting profile represents a lump centered at the origin now surrounded by six concentric rings.

In general, the magnetic field for $0 < \alpha < 1$ possesses a nonvanishing value B_0 (i.e. the magnitude of the lump) at the origin which eventually stand for the global maximum of the corresponding solution, see the results for both $\alpha = 0.25$ and $\alpha = 0.50$, for instance. Moreover, for intermediate values of r , the magnetic profile develops an intricate structure which now interpolates between six zeros and six peaks (which define each one of the concentric rings) before vanishing in the asymptotic limit.

In particular, based on the results in the tables I, II and III, it is possible to conclude that the positions of the first, third and fifth (second, fourth and sixth) zeros of the magnetic field move towards (outwards) the origin as α increases, with the positions of the rings inherent to its internal structure behaving in the very same way. In addition, the amplitudes of the first, third and fifth (second, fourth and sixth) peaks get higher (lower) as α increases.

c. The case $\alpha = 1$: The interested reader can follow this route in order to describe the shape of the magnetic field for different values of the parameter α . For instance, when $\alpha = 1$, Eq. (71) predicts the existence of four exact roots, but only two of them are located at intermediate values of r (while the other two roots are positioned at the boundaries). We therefore conclude that the corresponding magnetic solution presents two different zeros (beyond the ones located at $r = 0$ and in the asymptotics). In addition, the transcendental Eq. (72) leads to seven roots, but four of them are exactly the ones previewed by Eq. (71) itself, while the remaining three roots define the peaks (rings) which form the resulting internal structure. In summary, the magnetic solution for $\alpha = 1$ has a dramatically new profile which vanishes at $r = 0$ (i.e. $B_0 = 0$, see Eq. (73)) and presents an internal structure formed by three rings *without* a lump inside them.

d. The case $\alpha > 1$: On the other hand, when $\alpha = 1.5$ and $\alpha = 2$, Eq. (71) does not admit any solution, while Eq. (72) itself provides five (with a sixth one located at $r = 0$) approximate roots which stand for two local minima (not equal to zero) and three local maxima of $B(r)$, from which we infer the existence of an internal structure with a new profile whose interpolation does not include different zeros and therefore describes a configuration with three concentric volcanos.

As α increases, the number of roots (i.e. the number of minimums and maximums over which the internal structure interpolates) provided by the transcendental Eq. (72) decreases. The interested reader can verify that, when α is sufficiently large, that Equation does not support any root, from which the corresponding magnetic field stands for a single lump centered at the origin which vanishes monotonically in the asymptotic limit.

2. The BPS energy density

We end our manuscript by clarifying how the magnetic energy distribution changes with α when the magnetic permeability is given by Eq. (66). In this case, the magnetic energy density (38) can be written as

$$\varepsilon_{bps}^M = h^4 [\alpha - \cos^2(3\pi h)]^2, \quad (86)$$

where we have implemented our choices to both $\mathcal{W}(h)$ and $G(h)$, together with $g = \lambda = 1$, $\sigma = \beta = 2$ and $n = 3$.

As in the previous case, the Skyrme energy density (39) is again given by $\varepsilon_{bps}^S = h^2$ and therefore stands for a lump centered at $r = 0$ for all values of α (i.e. no significant variations to be considered).

On the other hand, to study the effects caused by the

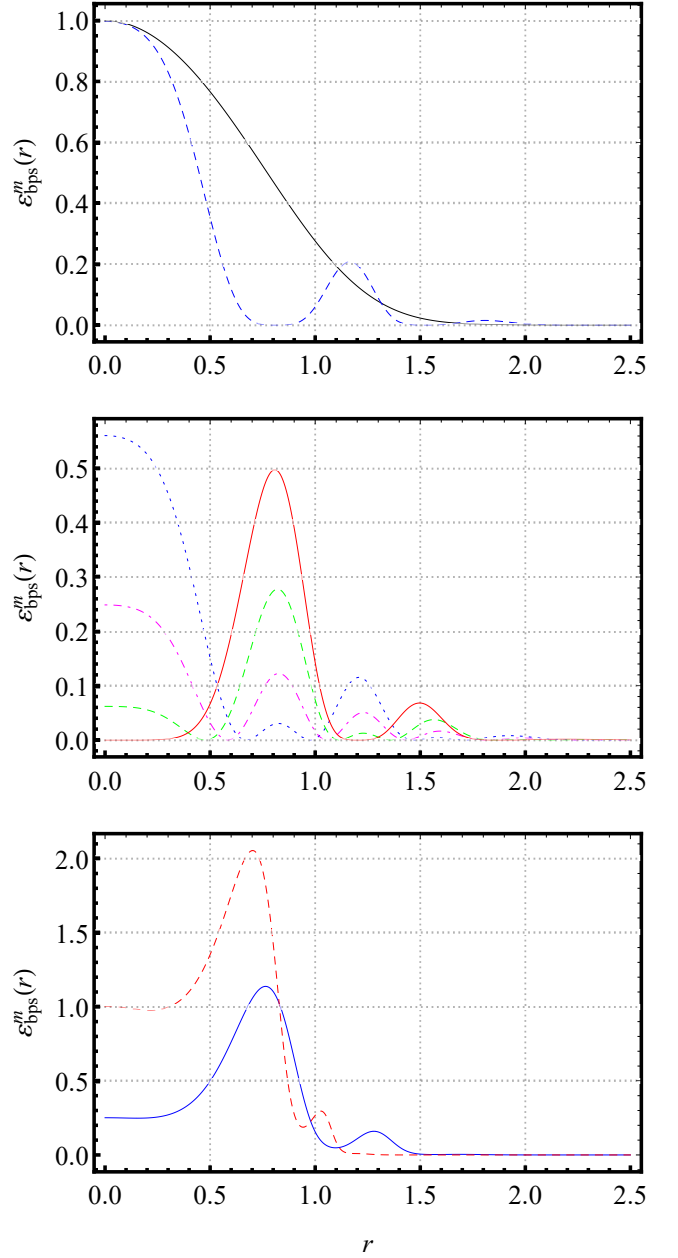


FIG. 12. Numerical solutions to the BPS magnetic energy density $\varepsilon_{bps}^M(r)$ obtained via Eqs. (67) and (68) for different values of α . Conventions as in the Fig. 9.

different values of α on the shape of ε_{bps}^M , we calculate

$$\begin{aligned} \frac{d}{dr} \varepsilon_{bps}^M &= 4h^3 [\alpha - \cos^2(3\pi h)] \\ &\times \left[[3\pi h \sin(3\pi h) - \cos(3\pi h)] \cos(3\pi h) + \alpha \right] \frac{dh}{dr} \end{aligned} \quad (87)$$

via which one gets that the condition $(\varepsilon_{bps}^M)' = 0$ gives rise to

$$\cos^2(3\pi h) = \alpha, \quad (88)$$

$$[3\pi h \sin(3\pi h) - \cos(3\pi h)] \cos(3\pi h) = -\alpha, \quad (89)$$

TABLE IV. Results for $\alpha = 0.25$. The exact roots of Eq. (88) (first column), the approximate roots of Eq. (89) (second column) and the values of $\varepsilon_{bps}^M(r)$ calculated at these last roots (third column). The magnetic energy density at the origin is given by $\varepsilon_{bps,0}^M = 0.5625$.

Roots of (88)	Roots of (89)	Values of ε_{bps}^M
8/9	0.8367	0.0304
7/9	0.6790	0.1153
5/9	0.5055	0.0040
4/9	0.3563	0.0080
2/9	0.1812	6×10^{-5}
1/9	0.0736	3×10^{-6}

where the first one is the same Eq. (71).

The value of the magnetic energy density at $r = 0$ can be verified to be

$$\varepsilon_{bps,0}^M = \varepsilon_{bps}^M(r=0) = (\alpha - 1)^2, \quad (90)$$

i.e. the same result obtained in the previous case, see the Eq. (65). Here, we have again used $h(r=0) = 1$.

From this point on, we implement the same prescription used previously, i.e. we solve Eqs. (88) and (89) for a particular α , from which we get the corresponding roots h_i 's. We then calculate ε_{bps}^M via Eq. (86) at those different h_i 's and categorize the resulting values as local maxima or minima of the solution, from which we interpret the magnetic energy density according to its profile and describe how its dimensions depend on α .

In what follows, we again consider only some ranges of values for α , for the sake of illustration.

a. The case $\alpha = 0$: It mimics the behavior already identified for the magnetic field itself, i.e. in this case, the Eq. (88) provides the roots given by Eqs. (75), (76) and (77). As explained previously, at these points, $B(r)$ vanishes identically, so as the magnetic energy density, from which we conclude that the resulting solution to $\varepsilon_{bps}^M(r)$ presents therefore 3 (three) different zeros.

In addition, Eq. (89) can be reduced to

$$[3\pi h \sin(3\pi h) - \cos(3\pi h)] \cos(3\pi h) = 0, \quad (91)$$

which is satisfied by $\cos(3\pi h) = 0$ (i.e. the Eq. (88) for $\alpha = 0$) and

$$3\pi h \sin(3\pi h) - \cos(3\pi h) = 0, \quad (92)$$

which stands for a transcendental expression whose roots must be determined numerically.

Once that we have obtained the roots of $\cos(3\pi h) = 0$ and clarified that they represent the zeros of ε_{bps}^M , we now focus our attention on the solutions of Eq. (92) above and their meaning concerning the magnetic energy profile.

The point is that the transcendental Eq. (92) admits three numerical roots given approximately by

$$h_1 = 0.6830, \quad (93)$$

$$h_2 = 0.3635, \quad (94)$$

$$h_3 = 0.0913, \quad (95)$$

from which one calculates the values $\varepsilon_{bps,1}^M = 0.2075$, $\varepsilon_{bps,2}^M = 0.0148$ and $\varepsilon_{bps,3}^M = 0.00001$, respectively, which stand for local maxima of the magnetic energy density. The solution to ε_{bps}^M obtained for $\alpha = 0$ therefore presents three different peaks for intermediate values of r .

Moreover, when $\alpha = 0$, the value of ε_{bps}^M at $r = 0$ can be verified to be

$$\varepsilon_{bps,0}^M = 1, \quad (96)$$

according to the previous Eq. (90).

In summary, the results above reveal that the magnetic energy's profile starts from its global maximum at $r = 0$ and then interpolates between three zeros and three peaks before vanishing in the asymptotic limit, the resulting solution forming a lump surrounded by three rings.

b. The case $0 < \alpha < 1$: In this case, Eq. (88) admits the 6 (six) analytical roots given by Eq. (85), from which one gets that ε_{bps}^M now possess six different zeros, this way mimicking the behaviour of $B(r)$ itself.

In addition, the approximate roots which come from the numerical study of Eq. (89) give rise to those peaks (rings) which define the internal structure inherent to the magnetic energy's profile, with the value of such energy density at $r = 0$ (i.e. the magnitude of the centered lump) still being given by Eq. (90).

Again for the sake of illustration, we solve the transcendental Eq. (89) for $\alpha = 0.25$, $\alpha = 0.50$ and $\alpha = 0.75$, from which we display the numerical results in the second columns of the tables IV, V and VI, respectively. These tables also bring the exact roots of Eq. (88) (i.e. the points at which ε_{bps}^M vanishes, see the first column) and the corresponding values of magnetic energy's peaks (third column).

The comparison between the results displayed in the tables IV, V and VI reveals that the solution to ε_{bps}^M for $0 < \alpha < 1$ has a nonvanishing value at $r = 0$ which only eventually represents a global maximum of the corresponding profile. In addition, driven by the magnetic field itself, the solution to ε_{bps}^M presents an internal structure with six zeros and six peaks, i.e. it stands for a lump now surrounded by six rings.

The results also show that both the zeros and the peaks (i.e. the position of the rings) of the magnetic energy density behave in the same way as those of $B(r)$ itself, i.e. as

TABLE V. Results for $\alpha = 0.50$. Conventions as in the Table IV. The magnetic energy density at the origin is given by $\varepsilon_{bps,0}^M = 0.25$.

Roots of (88)	Roots of (89)	Values of ε_{bps}^M
11/12	0.8400	0.1225
9/12	0.6749	0.0506
7/12	0.5109	0.0163
5/12	0.3490	0.0034
3/12	0.1933	0.0003
1/12	0.0571	6×10^{-7}

TABLE VI. Results for $\alpha = 0.75$. Conventions as in the Table IV. The magnetic energy density at the origin is given by $\varepsilon_{bps,0}^M = 0.0625$.

Roots of (88)	Roots of (89)	Values of ε_{bps}^M
17/18	0.8433	0.2778
13/18	0.6708	0.0125
11/18	0.5161	0.0375
7/18	0.3414	0.0008
5/18	0.2044	0.0007
1/18	0.0388	3×10^{-8}

α increases, the first, third and fifth (second, fourth and sixth) zeros and peaks of ε_{bps}^M move towards (outwards) the origin.

c. The case $\alpha > 1$: In addition, the solutions for $\alpha = 1.5$ and $\alpha = 2$ possess an internal structure which interpolates between different minima which are not equal to zero (multiple volcano configurations). As before, an increasing α continuously reduces the number of roots which solve Eq. (89). This number finally vanishes for α large enough. This extreme case (i.e. the absence of roots) gives rise to a magnetic energy distribution whose numerical curve forms a lump centered at $r = 0$ with no internal structure (i.e. it vanishes monotonically in limit $r \rightarrow \infty$).

IV. SUMMARY AND PERSPECTIVES

We have investigated BPS solitons inherent to a gauged baby Skyrme scenario in which a nontrivial function (which plays the role of the magnetic permeability of the medium) multiplies the Maxwell term. This enlarged model possesses a well-defined BPS structure which allows us to attain the self-dual equations and a lower bound for the total energy which is proportional to the topological charge, as expected. The convenient choice of the magnetic permeability function allows the construction of magnetic fields whose profiles dramatically differ from their standard counterparts.

We have focused our attention on those time-independent configurations with radial symmetry. This way, we have divided our investigation into two different branches according to the expression for the magnetic permeability (which depends on the parameter $\alpha \in \mathbb{R}$). We have solved the corresponding BPS equations numerically by means of a finite-difference scheme, from which we have observed that the profiles of the BPS solutions dramatically depend on α . We have then explained analytically the formation of internal structures based on the values of α . In the sequence, we have identified the effects caused by different values of α on the general shape of the numerical solutions, including the emergence of a sophisticated structure which interpolates between differ-

ent peaks (rings) and zeros of the BPS magnetic sector. We have also studied how the dimensions which distinguish such structures (such as amplitude and radius) depend on α itself.

Next, we have depicted the numerical solutions for different values of α and fixed values of the other constants of the model. The figures not only confirm our analytical predictions concerning the occurrence of internal structures and their dimensions, but they also allow us to observe how these structures can be extremely intricate depending on α itself. In this sense, we have pointed out that, when α is relatively small, the magnetic sector develops an structure formed by multiple concentric rings positioned at intermediate values of the radial coordinate. On the other hand, it is important to highlight that α sufficiently large leads to numerical solutions which mimic the canonical shape (differing from their standard counterparts only by their dimensions, such as amplitude and radius), i.e. a single lump with a compact profile centered at $r = 0$ and which therefore vanishes in the asymptotics.

The values of both the magnetic field and the magnetic energy density at the origin depend on α explicitly and this fact helps us to define how the corresponding profiles must be classified according to the position of their global maximums. Moreover, the lower bound for the total energy does not depend on α , being exactly the same for all the cases considered in the present manuscript.

We are currently studying the existence of BPS skyrmions in the context of a theory in which the dynamics of the gauge field is controlled by the Born-Infeld action now enlarged to include a nontrivial magnetic permeability, from which we expect the obtainment of BPS solutions with internal structures which can be thought as generalisations of the ones presented in this work. The results will be reported in a future contribution.

ACKNOWLEDGMENTS

The authors thank Prof. Dionísio Bazeia and Prof. Lukasz Stepien for motivating discussions. This work was financed in part by the Coordenação de Aperfeiçoamento de Pessoal de Nível Superior - Brasil (CAPES) - Finance Code 001, the Conselho Nacional de Pesquisa e Desenvolvimento Científico e Tecnológico - CNPq and the Fundação de Amparo à Pesquisa e ao Desenvolvimento Científico e Tecnológico do Maranhão - FAPEMA (Brazilian agencies). In particular, J. A. and A. C. S. thank the full support from CAPES (via a PhD scholarship and a Postdoctoral fellowship, respectively), R. C. acknowledges the support from the grants CNPq/306724/2019-7, FAPEMA/Universal-01131/17 and FAPEMA/Universal-00812/19, and E. H. thanks the support from the grant CNPq/309604/2020-6.

-
- [1] N. Manton and P. Sutcliffe, *Topological Solitons* (Cambridge University Press, Cambridge, England, 2004).
- [2] E. Bogomol'nyi, *Sov. J. Nucl. Phys.* **24**, 449 (1976). M. Prasad and C. Sommerfield, *Phys. Rev. Lett.* **35**, 760 (1975).
- [3] H. J. de Vega and F. A. Schaposnik, *Phys. Rev. D* **14**, 1100 (1976).
- [4] A. N. Atmaja, H. S. Ramadhan and E. da Hora, *J. High Energy Phys.* **1602**, 117 (2016).
- [5] K. Sokalski, *Acta Phys. Pol. A* **56**, 571 (1979); *Phys. Lett. A* **81**, 102 (1981). P. T. Jochym and K. Sokalski, *J. Phys. A* **26**, 3837 (1993). K. Sokalski, T. Wietecha and Z. Lisowski, *Acta Phys. Pol. B* **32**, 2771 (2001). K. Sokalski, L. Stepien and D. Sokalska, *J. Phys. A* **35**, 6157 (2002). L. Stepien, D. Sokalska and K. Sokalski, *J. Nonlinear Math. Phys.* **16**, 25 (2009).
- [6] T. H. R. Skyrme, *Proc. R. Soc. A* **260**, 127 (1961); *Nucl. Phys.* **31**, 556 (1962); *J. Math. Phys. (N. Y.)* **12**, 1735 (1971).
- [7] G. Adkins, C. R. Nappi and E. Witten, *Nucl. Phys. B* **228**, 552 (1983). G. Adkins and C. R. Nappi, *Nucl. Phys. B* **223**, 109 (1984). C. J. Halcrow, C. King and N. S. Manton, *Phys. Rev. C* **95**, 031303(R) (2017). C. Naya and P. Sutcliffe, *Phys. Rev. Lett.* **121**, 232002 (2018). I. Sharma, R. Kumar and M. K. Sharma, *Nucl. Phys. A* **983**, 276 (2019).
- [8] B. M. A. G. Piette, B. J. Schroers and W. J. Zakrzewski, *Z. Phys. C* **65**, 165 (1995); *Nucl. Phys. B* **439**, 205 (1995).
- [9] T. Gisiger and M. B. Paranjape, *Phys. Rev. D* **55**, 7731 (1997).
- [10] C. Adam, T. Romanczukiewicz, J. Sanchez-Guillen and A. Wereszczynski, *Phys. Rev. D* **81**, 085007 (2010).
- [11] S. L. Sondhi, A. Karlhede, S. A. Kivelson and E. H. Rezayi, *Phys. Rev. B* **47**, 16419 (1993). O. Schwindt and N. R. Walet, *Europhys. Lett.* **55**, 633 (2001). A. Neubauer, C. Pfeleiderer, B. Binz, A. Rosch, R. Ritz, P. G. Niklowitz and P. Böni, *Phys. Rev. Lett.* **102**, 186602 (2009). A. C. Balram, U. Wurstbauer, A. Wojs, A. Pinczuk and J. K. Jain, *Nat. Commun.* **6**, 8981 (2015). T. Chen and T. Byrnes, *Phys. Rev. B* **99**, 184427 (2019).
- [12] J. Fukuda and S. Zumer, *Nat. Commun.* **2**, 246 (2011). S. Kang, E.-W. Lee, T. Li, X. Liang, M. Tokita, K. Nakajima and J. Watanabe, *Angew. Chem. Int. Ed.* **55**, 11552 (2016).
- [13] A. A. Zyuzin, J. Garaud and E. Babaev, *Phys. Rev. Lett.* **119**, 167001 (2017).
- [14] Y. Kodama, K. Kokubu and N. Sawado, *Phys. Rev. D* **79**, 065024 (2009). Y. Brihaye, T. Delsate, N. Sawado and Y. Kodama, *Phys. Rev. D* **82**, 106002 (2010). T. Delsate and N. Sawado, *Phys. Rev. D* **85**, 065025 (2012).
- [15] S. Mühlbauer, B. Binz, F. Jonietz, C. Pfeleiderer, A. Rosch, A. Neubauer, R. Georgii and P. Boni, *Science* **323**, 915 (2009). X. Z. Yu, Y. Onose, N. Kanazawa, J. H. Park, J. H. Han, Y. Matsui, N. Nagaosa and Y. Tokura, *Nature (London)* **465**, 901 (2010).
- [16] J. Gladikowski, B. M. A. G. Piette and B. J. Schroers, *Phys. Rev. D* **53**, 844 (1996).
- [17] C. Adam, C. Naya, J. Sanchez-Guillen and A. Wereszczynski, *Phys. Rev. D* **86**, 045010 (2012). C. Adam, C. Naya, T. Romanczukiewicz, J. Sanchez-Guillen and A. Wereszczynski, *J. High Energy Phys.* **05** (2015) 155. C. Adam and A. Wereszczynski, *Phys. Rev. D* **95**, 116006 (2017).
- [18] R. Casana, A. C. Santos, C. F. Farias and A. L. Mota, *Phys. Rev. D* **100**, 045022 (2019).
- [19] R. Casana, A. C. Santos, C. F. Farias and A. L. Mota, *Phys. Rev. D* **101**, 045018 (2020).
- [20] R. Casana and A. C. Santos, *Phys. Rev. D* **104**, 065009 (2021).
- [21] S. Bolognesi and S. B. Gudnason, *Nucl. Phys. B* **805**, 104 (2008).
- [22] S. Bolognesi and W. J. Zakrzewski, *Phys. Rev. D* **91**, 045034 (2015).
- [23] C. Adam, J. M. Queiruga, J. Sanchez-Guillen and A. Wereszczynski, *J. High Energy Phys.* **05**, 108 (2013). J. M. Queiruga, *Phys. Rev. D* **92**, 105012 (2015).
- [24] M. Nitta and S. Sasaki, *Phys. Rev. D* **90**, 105002 (2014); *Phys. Rev. D* **91**, 125025 (2015). S. B. Gudnason, M. Nitta and S. Sasaki, *J. High Energy Phys.* **01**, 014 (2017).
- [25] J. M. Queiruga, *J. Phys. A* **52**, 055202 (2019).
- [26] J. Andrade, R. Casana, E. da Hora and C. dos Santos, *Phys. Rev. D* **99**, 056014 (2019).
- [27] D. Bazeia, M. A. Liao, M. A. Marques and R. Menezes, *Phys. Rev. Research* **1**, 033053 (2019).